Energy, Mines and Resources Canada | Energie, Mines et Ressources Canada

CANMET

Canada Centre for Mineral and Energy Technology | Centre canadien de la technologie des minéraux et de l'énergie

THE EFFECT OF WEAR ON CRACK FORMATION AND WORK HARDENING IN BAINITIC Cr-Mo RAIL STEEL WEAR DISKS, WITH AND WITHOUT MARTENSITE

D.M. FEGREDO, J. KALOUSEK* and E.F. CONNORS
METALLURGY SECTION and *WESTERN LAB. NRC, VANCOUVER, B.C.

SEPTEMBER 1982

MINERALS RESEARCH PROGRAM

32 pp

PHYSICAL METALLURGY RESEARCH LABORATORIES
REPORT: MRP/PMRL 82-60(TR)

PHYSICAL METALLURGY RESEARCH LABORATORIES

REPORT MRP/PMRL 82-60(TR)

THE EFFECT OF WEAR ON CRACK FORMATION AND WORK HARDENING IN BAINITIC Cr-Mo RAIL STEEL WEAR DISKS, WITH AND WITHOUT MARTENSITE

by

D.M. FEGREDO, J. KALOUSEK* and E.F. CONNORS

INTRODUCTION

The first progress report (1) of this project on rail wear details the reasons why it was undertaken and the experimental approach adopted. In summary, experiments are being done to determine the effects of microstructure and hardness on the wear resistance of an experimental Cr-Mo eutectoid steel. The performance of other steels will be evaluated later. Rough blanks are heat-treated at PMRL, finish-machined and subjected to wear tests in NRC, Vancouver. The wear machine simulates heavy-load, service conditions on a sharp curve. Worn disks are metallographically evaluated at PMRL.

The work related below describes experimental techniques and results on eight worn disks, tested to date.

EXPERIMENTAL METHODS

Worn disks are radially sectioned to produce ~1/2 in. thick (~12.7 mm) tapered slices. Slices from the first four disks that were tested were Ni-plated prior to mounting for metallographic examination to prevent edge-bevelling and thus rounding of the work surface profile. The following plating conditions were used:

Nickel(ous) carbonate	220 g/L
Sulphamic acid	370 g/L
Nickel chloride	15 g/L
Boric acid	40 g/L
Hydrogen peroxide (3%)	2 ml/L
Anode	Nickel
Current density (CD)	150-200 mA/cm^2

*Senior Research Officer, Tribology Section, Western Laboratory NRC, Vancouver, B.C. V6R 1P5

pH	3
Plating time	10 minutes
Temperature 50-60°C	

However, the second batch of four disks was mounted as-sectioned and the integrity of the edges was retained by careful technique. Mounting was done with the appropriate section exposed for subsequent polishing and etching.

Specimens were examined optically in a Leitz metallograph. Microhardness measurements were made on a Tukon microhardness tester using both Knoop (500 g load) and diamond pyramid (100 g load) indenters. Indentations were made at distances of $\geq$25 μm and $\leq$25 μm from the worn surface by the former and latter respectively.

Certain features of the wear test described in Reference 1 were amended slightly. The new test sequence is as follows:

(a) A constant load of 800 lb (363 kg) is used.

(b) Angles of attack of 10', 18', 36' and 40' are applied successively for 5000 revolutions. The machine stops for 2 min after every 20,000 revolutions, the disks reverse direction and the angles of attack change from a positive to a negative configuration that maintains the same high rail disk and simulates trains running in two directions on single line track.

(c) Dry or lubricated wear are alternated as follows in sets of 40K revolutions:

(i) First set (of 40K) run dry on virgin disks. Work hardening occurs, wear debris is collected and the test is interrupted to examine the profile.

(ii) Sets 2-20 are run lubricated. The test is interrupted and the profile examined.

(iii) Set 21 run dry. The test is interrupted, wear debris is collected and the worn profile examined.

(iv) Sets 22-failure are run lubricated but the test is interrupted for profile examination after the 60th, 100th and 140th sets (if the disks last that long without developing cracks and spalls).

EXPERIMENTAL RESULTS

The isothermal transformation conditions and corresponding hardnesses of various heat-treated blanks are given in Table 3 of Reference 1. These blanks are differentiated by being numbered from 1 to 20 and the Table is reproduced in this report as Table 1. Disk pairs (3,4) and (5,6) were tested

first. Unfortunately, these tests were invalidated by a machine malfunction. Nevertheless, sections from these pairs were Ni-plated, mounted, polished and optically examined to record crack characteristics and worn surface profiles.

Figures 1(a,b) and 2(a,b,c) are optical micrographs of section surfaces from disks "3" and "4" respectively, at low and higher magnifications. Disks "3" and "4" simulate high and low rails respectively, and gauge face (high rail) and tread (high and low rails) profiles are indicated in Figs. 1(a) and 2(a). Knoop microhardness indentations are seen in Figs. 1(a) and 2(a). Only a few surface cracks were observed, e.g., Fig. 1(b).

Figures 3(a,b,c) and 4(a,b) show sections of paired disks "6" and "5" which simulate high and low rails respectively. A greater number of surface cracks are seen in this pair, e.g. Figs. 3(c) and 4(b) than in the former pair (3,4) but cracking was not prolific even at the gauge face, e.g., Fig. 3(b).

Valid wear tests were carried out on disk pairs (7,8) and (11,12). These were prepared for metallographic examination without Ni-plating.

Figures 5(a-d), 6(a-i), 7(a-h) and 8(a-k) illustrate section surfaces from disks "7", "8", "11" and "12" respectively. Figures 5(a), 6(a), 7(a) and 8(a) are photographs taken at low magnification (x14) and show worn surface profiles. Figures 5(b-d), 6(b-i), 7(b-h) and 8(b-k) are photographs at x500 and, except for Fig. 7(b-h), are of successive points from right to left along the worn surfaces shown in Figs. 5(a), 6(a) and 8(a). Figure 7(b-h) shows successive points from left to right along the surface shown in Fig. 7(a).

Microhardness values at different distances from the surfaces of the various disks are given in Table 2(a,b).

DISCUSSION

A schematic of wheel/rail interaction on a curve is presented in Fig. 9 (2) to illustrate the simulation effects attempted by the laboratory wear machine. Figure 9(a) shows that contact mainly occurs on the gauge side and up to the rail tread centre in the high rail whereas contact takes place in the low rail on the part of the tread extending from the centre to the field side, Fig. 9(b). Arrows on Fig. 9(a) and 9(b) point to locations "A", "B", "C" and "D" at which microhardness measurements were taken on the various disks with the diamond pyramid indenter. Figures 1(a) and 3(a) have the gauge face on the left-hand side of the (high rail) disk profiles, and Fig. 2(a) and 4(a) show the field side on the left of the (low rail) disk profiles.

The optical observations and microhardness measurements made at various depths below the worn surfaces of paired disks (3,4) and (5,6) are briefly discussed because these tests were invalid as mentioned above. These disks have upper bainitic microstructures and macro hardnesses (Rockwell tester) of ~Rc 45 and ~Rc 42 respectively (Table 1). The following observations were made:

(a) Similar worn profiles are observed in the two "high rail" disks "3" and "6" and in the two "low rail" disks "4" and "5". One of the objectives of these experiments is to determine whether wear properties are significantly affected by hardness for the same basic microstructure and these results imply similar wear rates in the two upper bainite microstructures for hardnesses of Rc 45 and Rc 42 respectively.

*(b) Inclusions are found within cracks and are illustrated by arrows in Fig. 1(b) and 3(c). The inference is that they play an important role in propagating and possibly initiating cracks. Furthermore, individual cracks or weakened zones formed at inclusions prior to cracking, e.g., chain brackets, Fig. 3(c), will tend to connect as wear continues and this process will be assisted if inclusions are aligned in rows by movement of the matrix through shear at and near the surface. Figures 2(b) and (c) show inclusions at the Ni plate-steel junction indicating that the worn pieces that flaked off there contained these inclusions on their cracked surfaces while the flakes were still part of the disk.

(c) A hardness gradient is observed very close to the worn surface, depending on location, as measured by the diamond pyramid indenter. In this connection it must be remarked that the interior of all specimens which show relatively undisturbed microstructures, consistently indicate hardnesses which increase in the order diamond pyramid: Rockwell tester: Knoop indenter. Of these three, the diamond pyramid indenter under a 100 g load indents very localized regions. However, a layered deformed region exists within 150-200 μm of the worn surface which, because of the very high squeezing effect, should be more homogeneous than coarse undeformed regions. Bearing this in mind, it appears that high hardness gradients occur in the first 25 μm depth below the worn surfaces in the two "high rail" disks "3" and "6" at (i) locations "C" and "D" for disk "3" and (ii) "A", "B", "C" and "D" for disk "6", Table 2(a). According to Fig. 9(a), locations "B", "C" and "D" should be basically affected. Relatively uniform hardnesses occur at greater depths (Knoop indenter). With regard to

*See note at end of text.

the "low rail" disks "4" and "5", high hardness gradients occur in the first 25 μm depth from the worn surface at (i) locations "A", "C" and "D" for disk "4" and (ii) locations "A", "B" and "C" for disk "5", Table 2(a). Figure 9(b) indicates that major hardness effects should occur in the surface region joined by points "A" and "B". The Knoop values again show that relatively uniform hardnesses occur at greater depths from the worn surfaces.

Paired disks (7,8) and (11,12) are also bainitic with hardnesses of ~Rc 42 and ~Rc 38 respectively. A comparison of the low magnification micrographs, of the "high rail" disks "7", Fig. 5(a) and "11", Fig. 7(a), indicates greater wear on the gauge face of disk "11" implying a possible effect of hardness on wear resistance. The diamond pyramid hardness values, Table 2(b), show high hardness gradients within 25 μm of the worn surfaces of these disks at (i) locations "B", "C" and "D" for disk "7" and (ii) locations "B" and "C" for disk "11". Lower hardness values are obtained at greater depths from the worn surfaces as indicated by the Knoop readings. The highest hardness values are obtained at location "B" in both "low rail" disks "8" and "12". These values are fairly uniform within the initial 25 μm depth and then diminish with distance as shown by the Knoop readings. These observations are essentially consistent with the wheel/rail contact zone of Fig. 9(b) and indicate that the objective of simulating wheel/rail contact in curved service is basically achieved for these pairs of disks.

High work hardening resulting in high hardness values thus occurs very close to the worn surface although, in the optical microscope, Fig. 5-8 show what appears to be the same type of sheared layer structure extending down to ~150-200 μm depths from the surface. This is explained by recent TEM work (3) that indicates that grains as fine as 10 nm are formed at the worn surface, the general direction of the carbides is parallel to the worn surface down to a depth of 20 μm and the inter-carbide spacing varies from ~25 nm at the worn surface to ~70 nm at 20 μm depth, compared to ~100-140 μm in the undeformed material. Presumably, high work hardening occurs very near the surface because the simulated wheel/rail interaction forces are either more complex there or have a much greater intensity. Tensile tests, Table 3, demonstrate that the bainitic structures of all disks have large YS/UTS ratios, i.e., low tensile work hardening characteristics, and that tensile deformation does not significantly increase the microhardness.

Figures 5 and 6 of the disk pair (7,8) show cracks associated with inclusions, e.g., Fig. 5(c), 5(d), 6(c), (d), (f) and (g). A few light-etching bands are visible near the surface in both disks, e.g., Fig. 5(d) and Fig. 6(c)-(f). These bands represent transformations that must have occurred, possibly in segregated regions, when the disks were cooling after isothermal transformation (salt-bath) treatment. Preliminary work (1) on thin slices had given times for ~100% transformation at particular temperatures and these conditions were applied to the disks. However, it appears that longer times are necessary for the latter and fresh blanks have been heat-treated for increased times to ensure full bainitic transformation. Martensite is visible as discrete, unsheared entities in the light-etching bands, e.g., Fig. 6(e) and (f). The bands, in general, must be bainitic as microhardness measurements on disk (8) [Note in Table 2(b)] indicate they have a hardness of Rc 46 while the matrix registers Rc 43. The association of cracks with these harder bands is marked, Fig. 6(d)-(g). Inclusions within these bands would also contribute to crack initiation and/or propagation. However, cracks may also form elsewhere and Fig. 6(c) shows a crack at an inclusion row in the matrix.

Figures 7 and 8 show that martensite occurs to a greater extent in disks "11" and "12" than in pair (7,8). The tests of these mixed martensite-bainite structures, although fortuitous, were instructive because of their relevance to wheel/rail interactions in rail welds which contain martensite. An examination of Fig. 7 and 8 reveals many examples in which cracks are associated with discrete pieces of martensite, e.g., Fig. 7(f) and (g) and Fig. 8(d), (e), (g) and (h). These very hard (~Rc 65) pieces remain undeformed even in the zones of intense shear at and near the worn surface. The layered bainite matrix appears to flow around the martensite, Fig. 7(f) and Fig. 8(d), (g) and (i) and aligns the pieces into rows along the general shear direction as if they are large inclusions, Fig. 7(d), (e), (f), and Fig. 8(f)-(j). The associated cracks seem to occur at (i) the martensite-bainite interface, e.g., Fig. 7(f) and Fig. 8(g)-(i), so that interface decohesion can accompany matrix deformation and lead to crack propagation and (ii) between pieces of martensite, e.g., Fig. 7(g) and Fig. 8(d), (e), (h), (i) and (j). In this case there is the possibility of the fracture of larger martensite pieces producing cracks. However, these cracks do not extend to the same degree as the decohesion cracks either because they are not in the intense surface shear zone, Fig. 7(f) and Fig. 8(e) and (h) or are partially shielded by the broken martensite halves, Fig. 8(d), (i) and (j).

REFERENCES

1. Fegredo, D.M. and Connors, E.F. "Progress report on the resistance to wear of selected commercial and experimental steels"; Division Report MRP/PMRL 81-27(TR), CANMET, Energy, Mines and Resources Canada; 1981.

2. Kalousek, J. "Track/train dynamics Report #4, Rail corrugations"; Canadian Pacific Dept. of Research, Report No. S488-75; p 54; February 1975.

3. Laufer, E.E. Interim Report No. 3 "TEM study on the effects of simulated rail loading on an experimental premium rail steel"; CANMET, Energy, Mines and Resources Canada; Contract 20SU.23440-0-9191; July 31, 1982.

NOTE: Optical work could only be done at this time. Detailed SEM observations will be obtained on these and other specimens.

Table 1. Salt-bath temperatures, time of immersion and average hardness (Rc) obtained on trial blanks and other blanks intended for wear tests. The blanks intended for wear tests are numbered 1 to 20 and individual numbers are given in parentheses. Hardness measurements done on surface illustrated in Fig. 1(b) in Ref. (1).

Salt-bath temp. °C	Time of immersion minutes	Average hardness (Rc) on trial blanks (TB) and blanks for wear tests. Latter are numbered from 1 to 20 and are given in parentheses.				
375	40	(TB)* 45	(1) 46	(2) 45	(3) 46	(4) 46**
415	40	(TB) 42	(5) 42	(6) 42	(7) 42	(8) 41.5**
460	45	(TB) 38	(9) 37.5	(10) 36.5	(11) 37	(12) 38**
627	30	(TB)† 38.5	(13) 38.5	(14) 38.5	(15) 36	(16) 38††
595	35	(TB) 42	(17) 42	(18) 42	(19) 42	(20) 41.5††

* Trial blank heat-treated at 380°C, not 375°C.

**Test Blanks numbers 1 to 12 had 0.020 in. (0.051 mm) ground from the surface and hardness measurements taken.

† Trial blank heat-treated at 620°C, not 627°C.

††Test blanks numbers 13 to 20 had 0.040 in. (0.10 mm) ground from the surface and hardness measurements taken.

Table 2(a). Avg. microhardness (Rc) at the distances (μm) indicated from the worn surface.

Disk	Diamond (100 g load)						Knoop (500 g load)					
	0	5	10	15	25	Location	25	50	250	1000	2000	Location
						Fig. 1(a) - Arrows						Fig. 1(a) - See indentations
3	45.3	45.3	46.9	46.9	43.6	"A" corner, field side	47		46.5	48	48.5	Avg on running surface
high	41.8	41.8	40.8	39.8	36.6	"B" centre of running surface		56	47.5	48	46	Gauge corner
rail	49.8	49.8	57.8	49.8	43.6	"C" gauge corner		46.5	48.5	48.5	47.5	Gauge face
	53.0	49.8	46.9	46.9	44.5	"D" gauge face						
	Interior hardness: Rockwell Machine Rc 44.5; Knoop Rc 47.75; DPH Rc 39											
						Fig. 2(a) - Arrows						Fig. 2(a) - See indentations
4	50.5	49.1	47.7	46.9	43.6	Corner "A" field side	49.5		48.5	49.5	49	Avg of running surface
low	42.7	41.8	42.7	44.5	41.8	"B" centre of running surface						
rail	55.7	55.7	49.8	46.9	44.5	Corner "C" gauge side						
	45.3	43.6	41.8	40.8	40.8	"D"						
	Interior hardness: Rockwell machine Rc 44; Knoop Rc 47; DPH Rc 41											
						Fig. 3(a) - Arrows						Fig. 3(a) - See indentations
6	47.7	46.9	43.6	43.6	35.5	"A" corner, field side	49	48	44.5	44.5	45	Avg on running surface
high	54.7	53	53	53	49.8	"B" centre of running surface	45		44	45.5	43	Gauge corner
rail	47.7	43.6	43.6	40.8	40.8	"C" gauge corner	50		42.5	43.5	44.5	Gauge face
	54.1	54.1	54.1	53	49.8	"D" gauge face						
	Interior hardness: Rockwell machine Rc 42; Knoop Rc 43; DPH Rc 37											
						Fig. 4(a) - Arrows						Fig. 4(a) - See indentations
5	49.8	49.3	48.4	48.4	46.9	"A" corner field side	48.5	47	44	45	45.5	Avg of running surface
low	53	53	49.8	43.6	40.8	"B" centre of running surface						
rail	49.8	49.8	49.8	46.9	46.9	"C" corner, gauge side						
	40.8	40.8	35.5	35.5	35.5	"D"						
	Interior hardness: Rockwell machine Rc 42; Knoop Rc 44; DPH Rc 38											

Table 2(b). Avg microhardness (Rc) at the distances (μm) indicated from the worn surface.

Disk	Diamond (100 g load)						Knoop (500 g load)					
	0	5	10	15	25	Location	25	50	250	1000	2000	Location
						Fig. 3(a) - Arrows						Fig. 5(a) - See indentations
7	38.8	38.8	38.8	35.5	34.4	"A" corner, field side						
high	51.7	49.8	49.8	49.8	46.9	"B" centre of running surface	48		46	46		Avg of running surface
rail	53	51.7	46.9	42.7	45.3	"C" gauge corner	49		45	46		Gauge corner
	49.9	46.9	46.9	41.8	41.8	"D" gauge face	40,38,33		44.8	44.8		Gauge face
	Interior hardness: Rockwell machine Rc 42; Knoop Rc 46; DPH Rc 36											
						Fig. 4(a) - Arrows						Fig. 6(a) - See indentations
8	43.6	42.7	43.6	39.8	40.8	"A" corner, field side						
low	49.8	46.9	46.1	46.1	46.9	"B" centre of running surface	48.5		48	46.5		Avg of running surface
rail	40.8	40.8	40.8	39.8	37.7	"C" corner, gauge side						
	34.4	34.4	34.4	35.4	34.4	"D"						
	Interior hardness: Rockwell machine Rc 41.5; Knoop Rc 46† 43†; DPH Rc 34.5 in matrix.											
						Fig. 3(a) - Arrows						Fig. 7(a) - See indentations
11	38.8	40.8	35.5	35.5	35.5	"A" corner, field side						
high	46.9	43.6	43.6	46.9	46.9	"B" centre of running surface	49.5		44.5	41		Avg on running surface
rail	53	53	49.8	49.8	49.8	"C" gauge corner	49		45.5	42.5		Gauge corner
			35.5	35.5	35.5	"D" gauge face	34,36,41		39	40.7		Gauge face
	Interior hardness: Rockwell machine Rc 37; Knoop Rc 43; DPH Rc 35.5											
						Fig. 4(a) - Arrows						Fig. 8(a) - See indentations
12	40.8	40.8	37.7	37.7	40.8	"A" corner, field side						
low	49.8	49.8	49.8	49.8	49.8	"B" centre of running surface	48.5		44	40.5		Avg of running surface
rail	40.8	40.8	37.7	40.8	40.8	"C" corner, gauge side						
	35.5	35.5	35.5	35.5	35.5	"D"						
	Interior hardness: Rockwell machine Rc 38; Knoop Rc 41.5; DPH Rc 35.5											

†Microhardness value within light-etching bands, Fig. 6(a), ~Rc 46; between bands ~Rc 43.

Table 3.

Tensile specimen Microstructure* equivalent to discs	YS MPa	UTS MPa	Ratio YS/UTS	El %	R.A %	Microhardness* (Rc) in broken tensile		Originalt Tensile Microhardness* Rc
						At fracture	in gauge length	
3,4	1353	1480	0.91	7	20	45	46	48.5
5,6,7,8	1175	1325	0.89	8	20	44	43.5	44
11,12	965	1165	0.83	8	18	40	40	41

*Microhardness obtained with 500 gram load.

†Determined on tensile specimen shoulders.

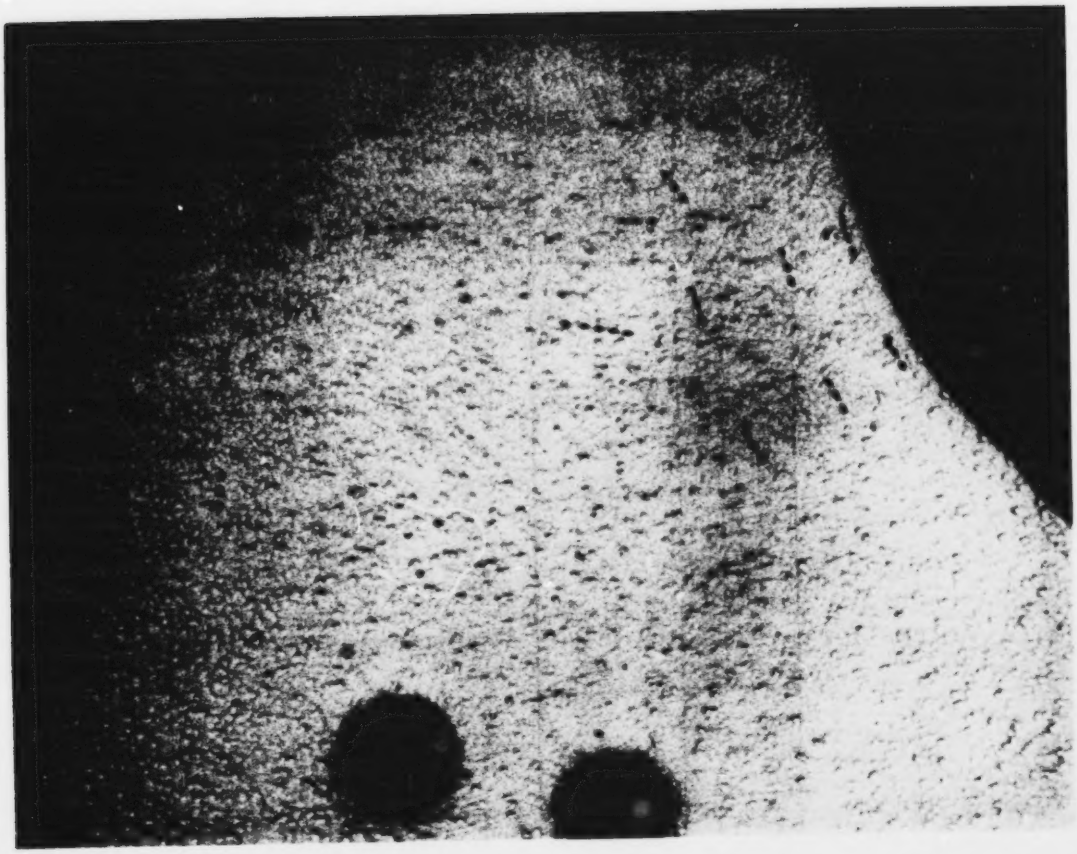

(a) X14 (neg 8313)

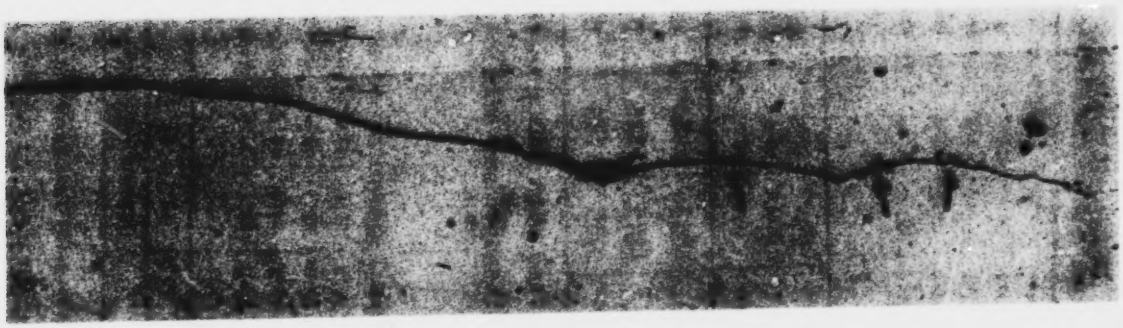

(b) X133 (neg 8314)

Fig. 1(a,b). Disk "3" (high rail). Arrows point to inclusions within cracks.

(a) x14 (neg 8315)

(b) x300 (neg 5766)

(c) x500 (neg 8316)

Fig. 2(a,b,c). Disk "4" (low rail).

Note: Inclusions at interface of steel and nickel plate.

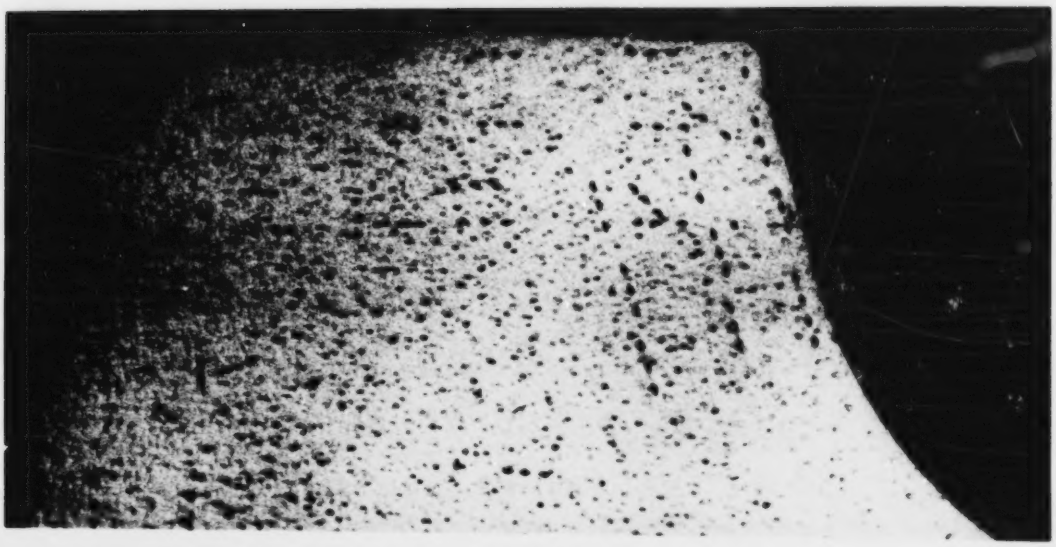

(a) x 14 (neg 8317)

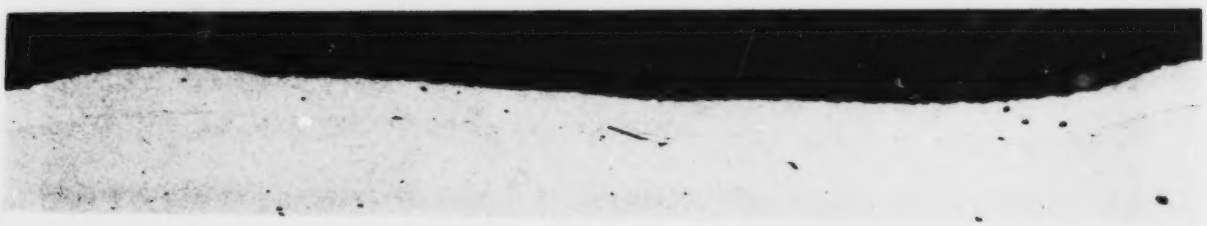

(b) Gauge face x100 (neg 8318)

(c) x400 (neg 8319)

Fig. 3. Disk "6" (high rail). Arrows point to inclusions. Chain brackets enclose inclusion rows.

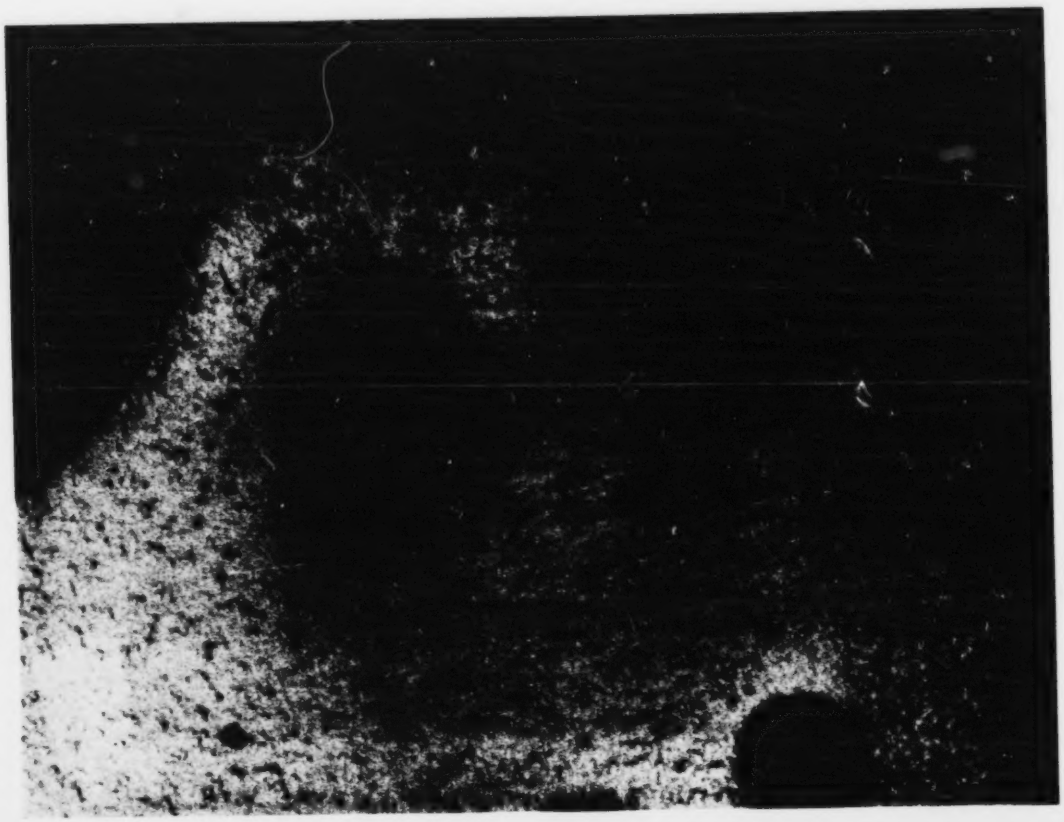

(a) x14 (neg 8320)

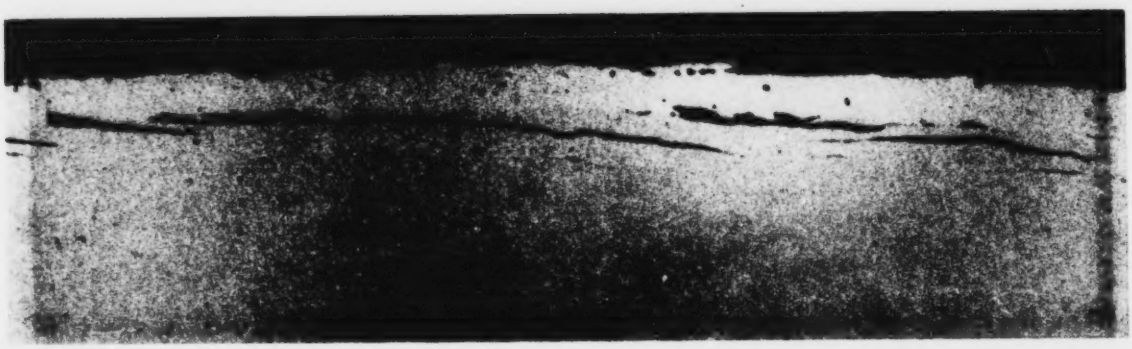

(b) x150 (neg 5767)

Fig. 4(a,b). Disk "5" (low rail).

(a) x14 (neg 8321)

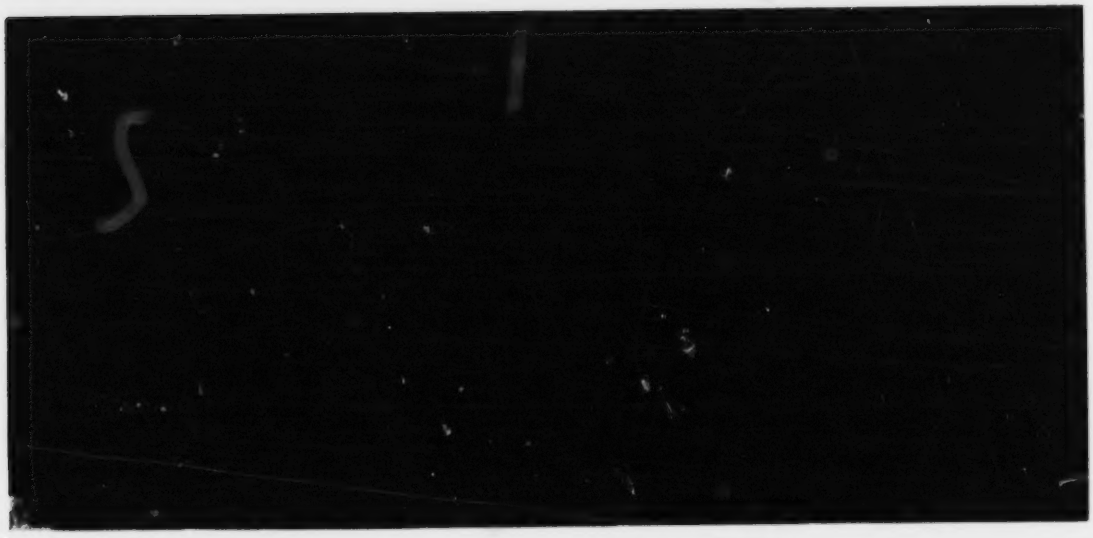

(b) x500 (neg 8322)

Fig. 5(a,b). Disk "7" (high rail).

(c) x500 (neg 8323)

(d) x500 (neg 8324)

Fig. 5(c,d). Disk "7" (high rail). Chain brackets enclose cracks which appear to be associated with inclusions.

(a)

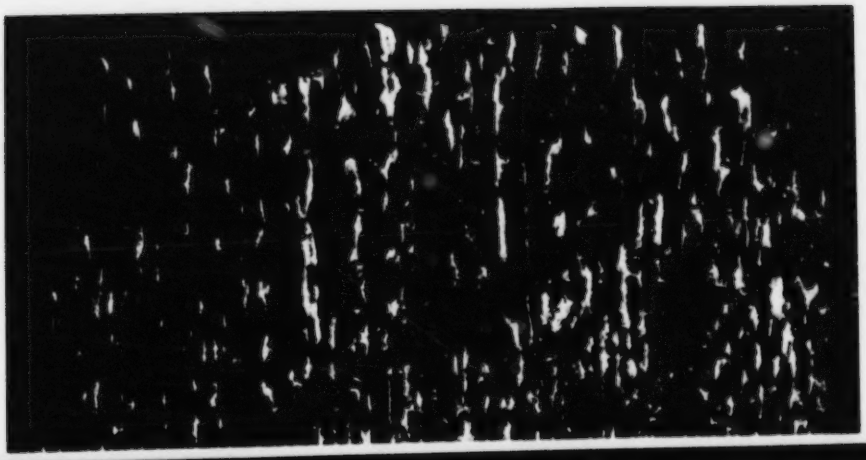

(b)

(c)

Fig. 6. Disk "8" (low rail). X500. Chain bracket encloses crack which is not in a light-etching band. (negs (a) 8325, (b) 8326, (c) 8327)

(d)

(e)

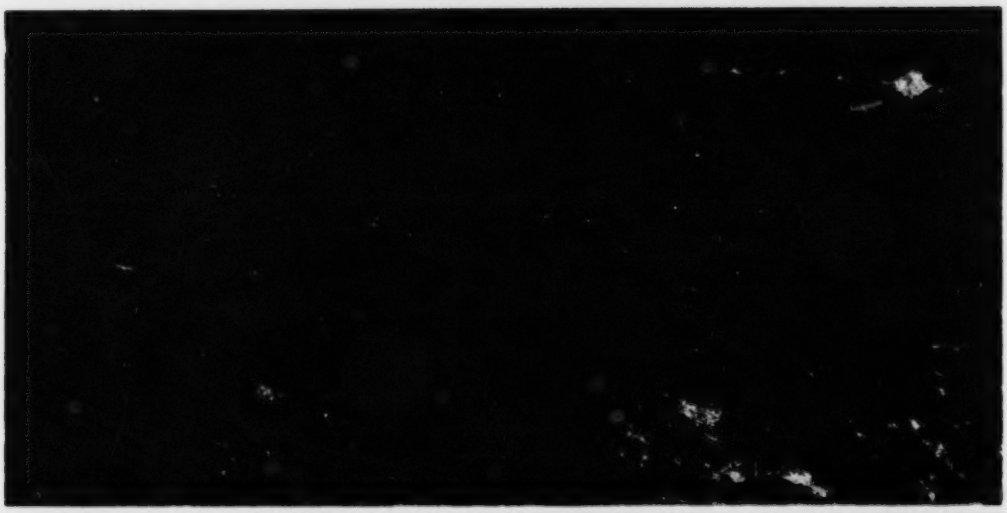

(f)

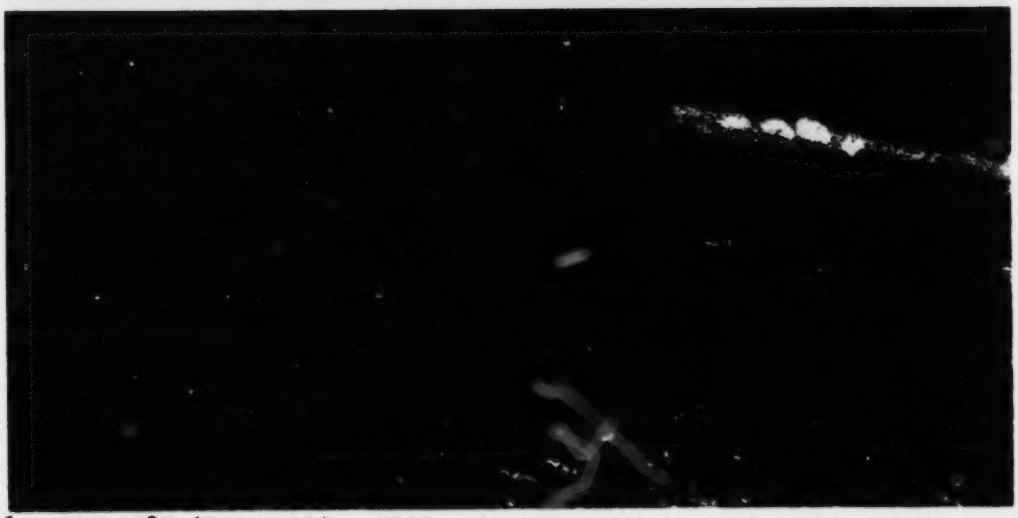

Fig. 6. Disk "8" (low rail). X500. Arrows point to inclusions within cracks which are in light-etching bands. (negs. (d) 8328, (e) 8329, (f) 8330)

(g)

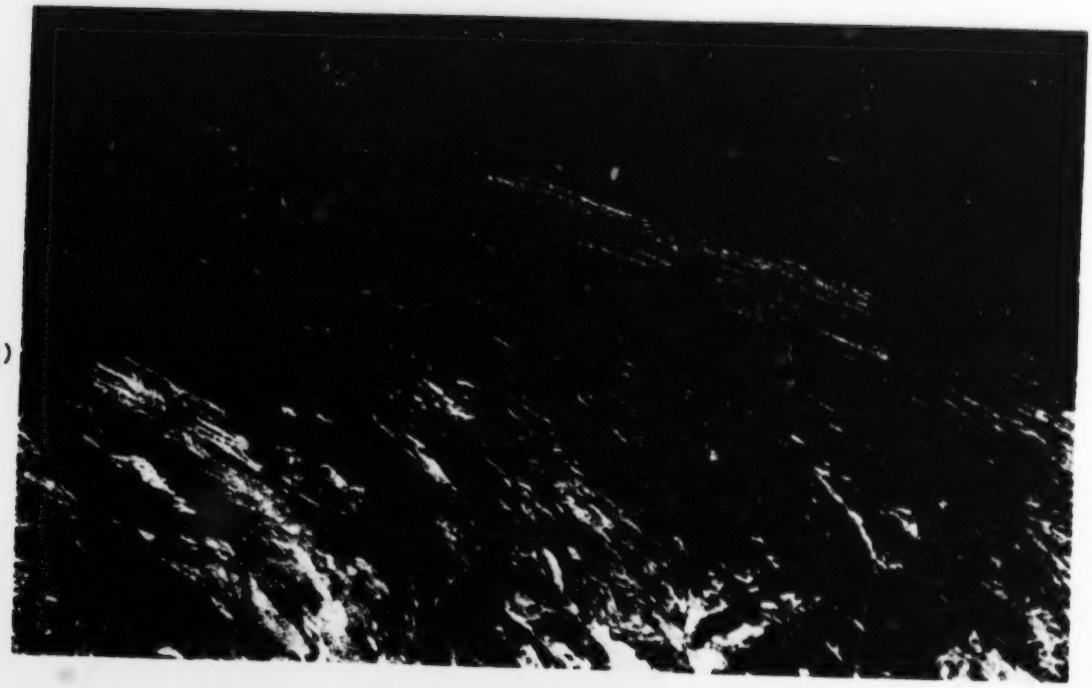

(h)

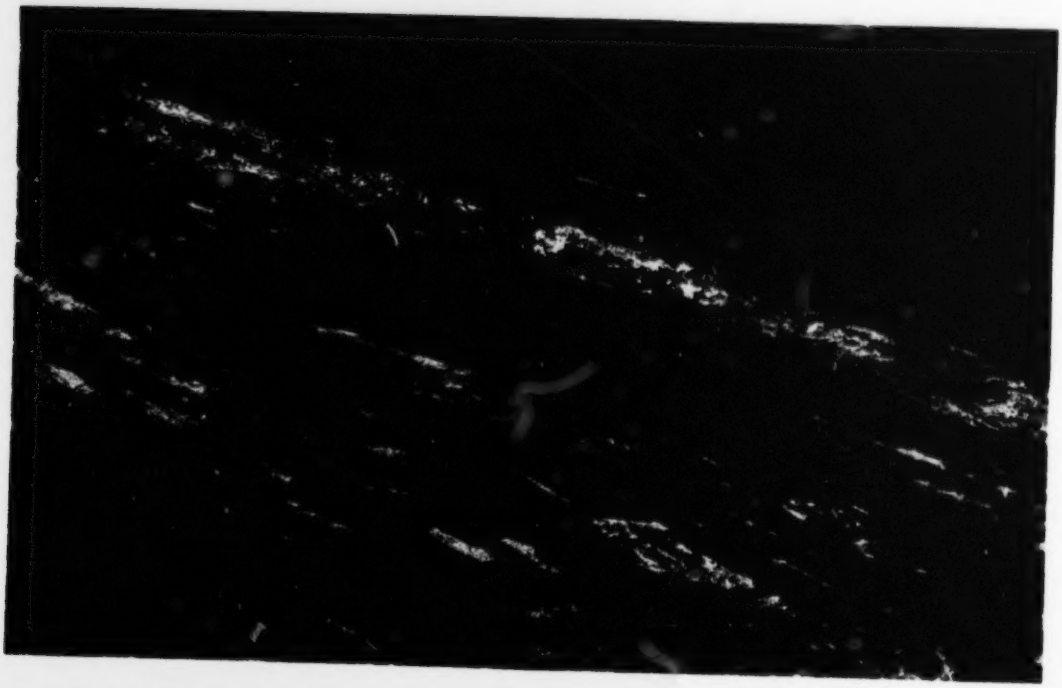

Fig. 6. Disk "8" (low rail). X500. Arrows point to inclusions within cracks which are in a light-etching band. Chain brackets enclose cracks. (negs. (g) 8331) and (h) 8332)

(i)

Fig. 6. Disk "8" (low rail). X500. (neg 8333)

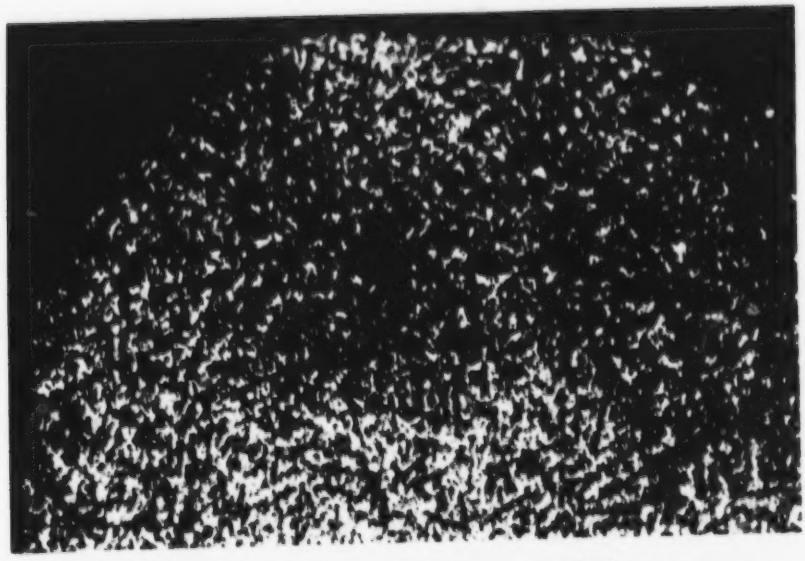

(a) X14 (neg 8334)

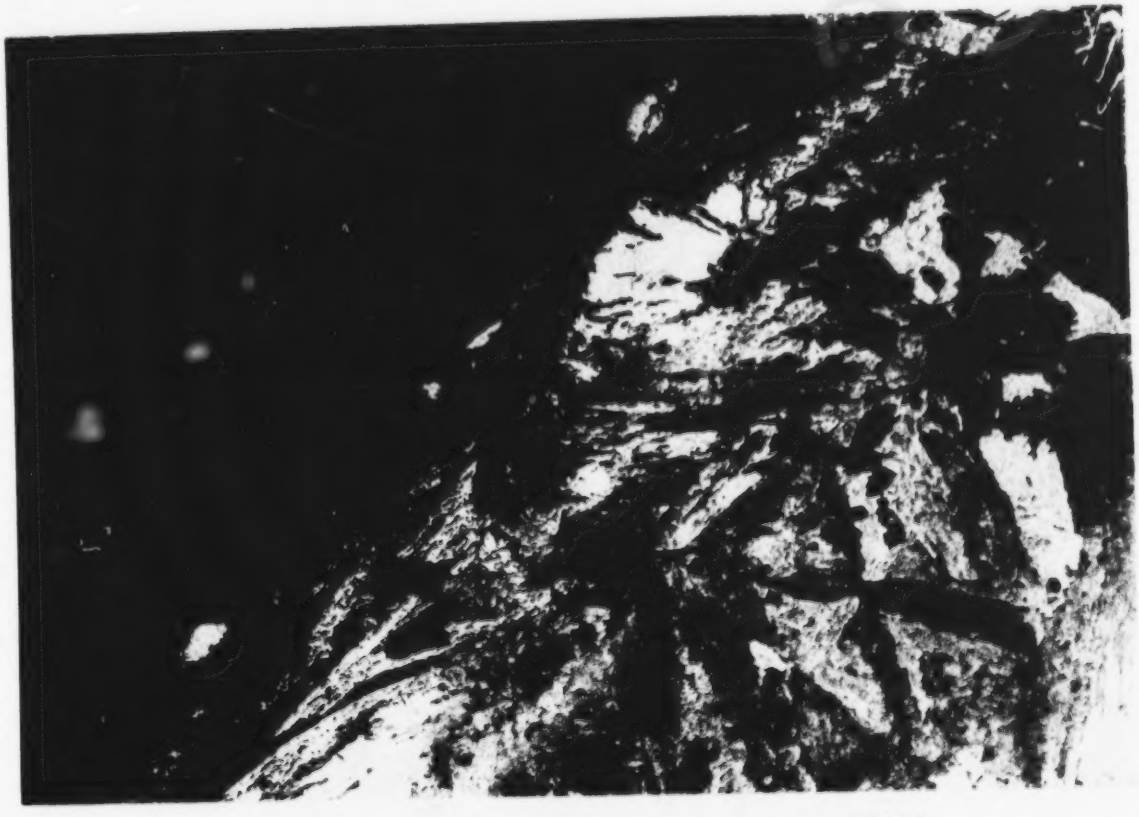

(b) Gauge face X500 (neg 8335)

Fig. 7. Disk "11" (high rail). (cont'd)

(c)

(d)

(e)

Fig. 7. Disk "11" (high rail). X500. Chain brackets in (d) and (e) enclose martensite rows. (cont'd) (negs. (c) 8336, (d) 8337, (e) 8338)

Fig. 7(f). Disk "11" (high rail). X500. Arrows above point to cracks associated with martensite. (neg 8339)

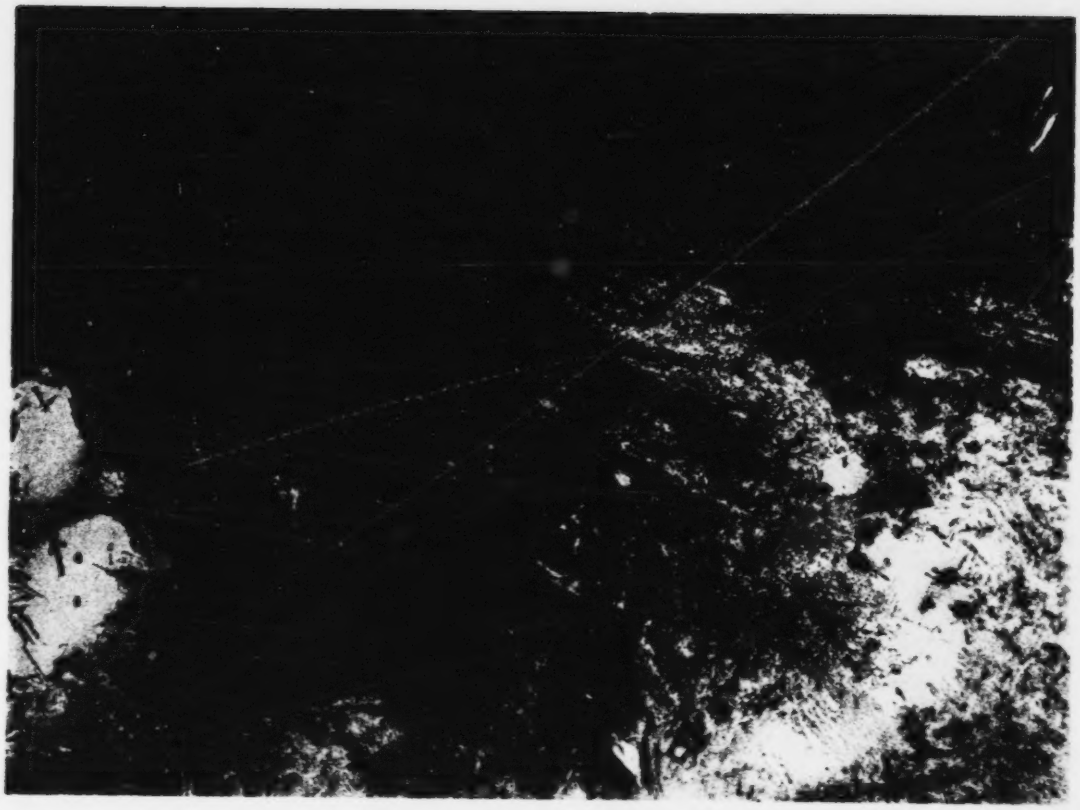

(g) (neg 8340)

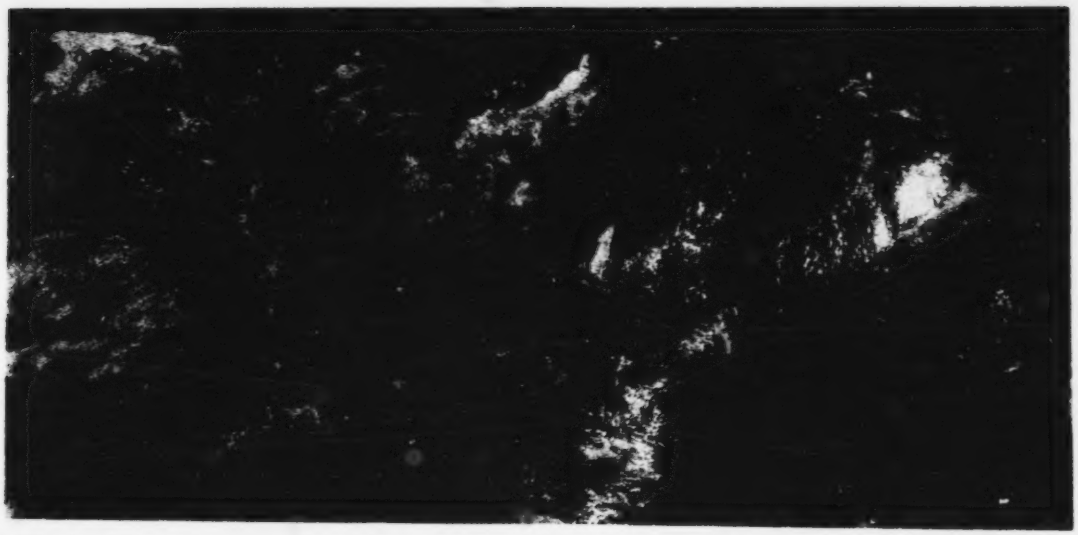

(h) (neg 8341)

Fig. 7. Disk "11" (high rail). X500. Arrows point to cracks associated with martensite.

(a)

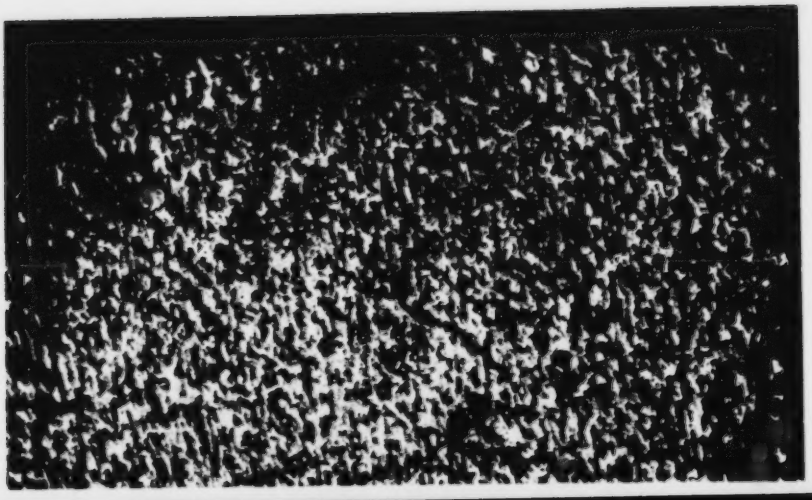

(b)

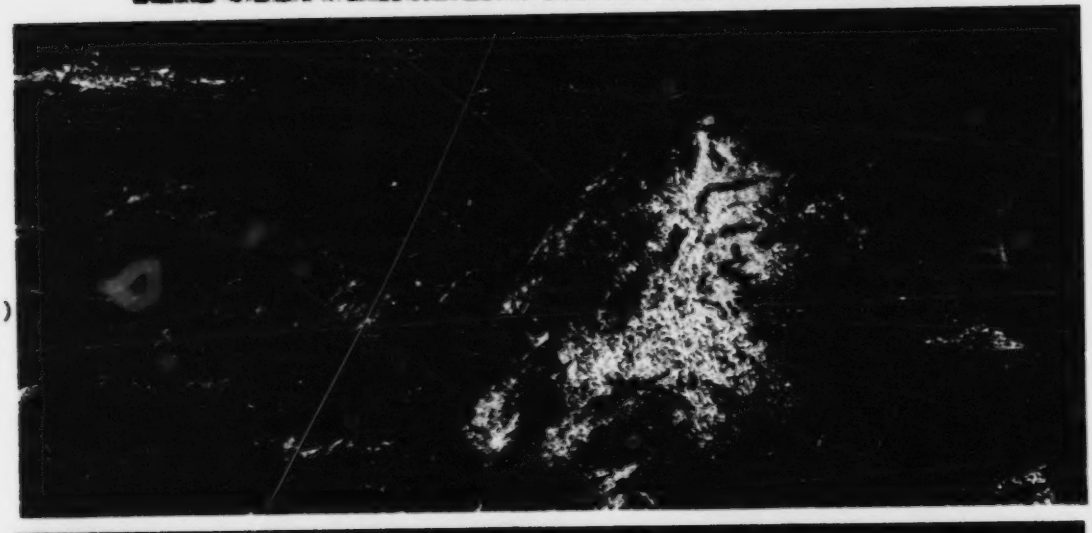

(c)

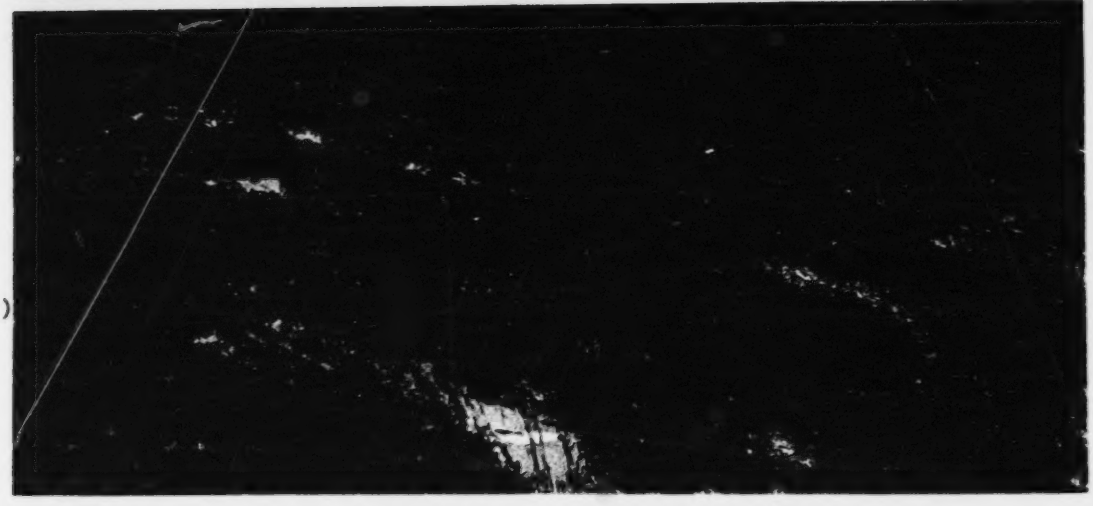

Fig. 8(a,b,c). Disk "12" (low rail). (a) X14, (b,c) X500 cont'd. (negs. (a) 8342, (b) 8343, (c) 8344)

(d)

(e)

Fig. 8(d,e). Disk "12" (low rail). X500. (e) directly below (d). Arrows point to cracks associated with martensite. Chain bracket encloses crack not associated with martensite block. (negs. (d) 6265, (e) 6266)

(f)

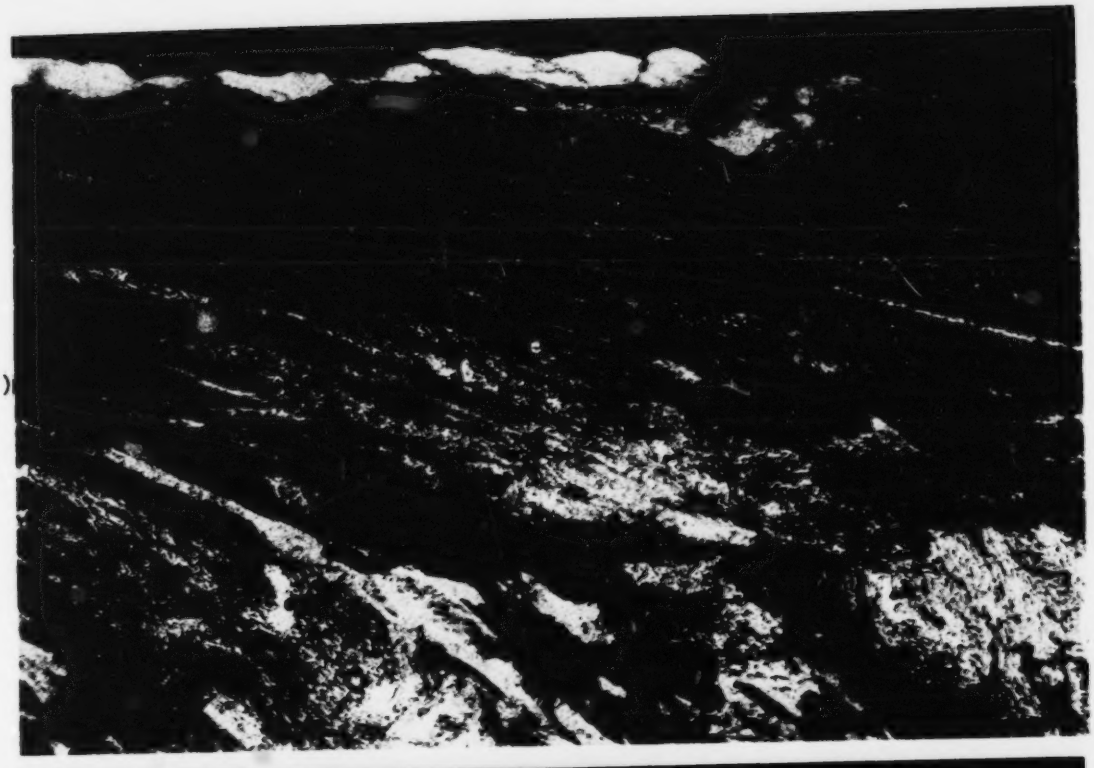

(g)

Fig. 8(f,g). Disk "12" (low rail). X500. Arrows point to cracks associated with martensite. (negs (f) 8345, (g) 8346)

(h)

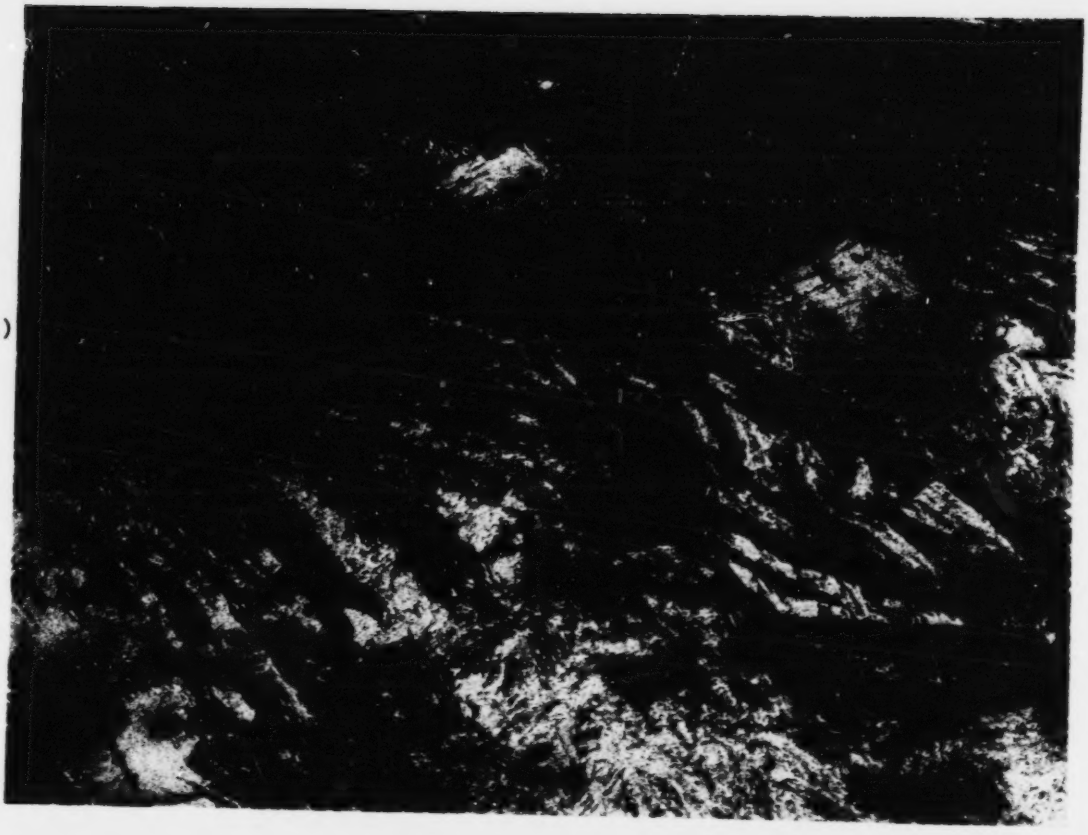

(i)

Fig. 8(h,i). Disk "12" (low rail). X500. Arrows point to cracks associated with martensite. Chain brackets enclose martensite rows. (negs (h) 8347, (i) 8348)

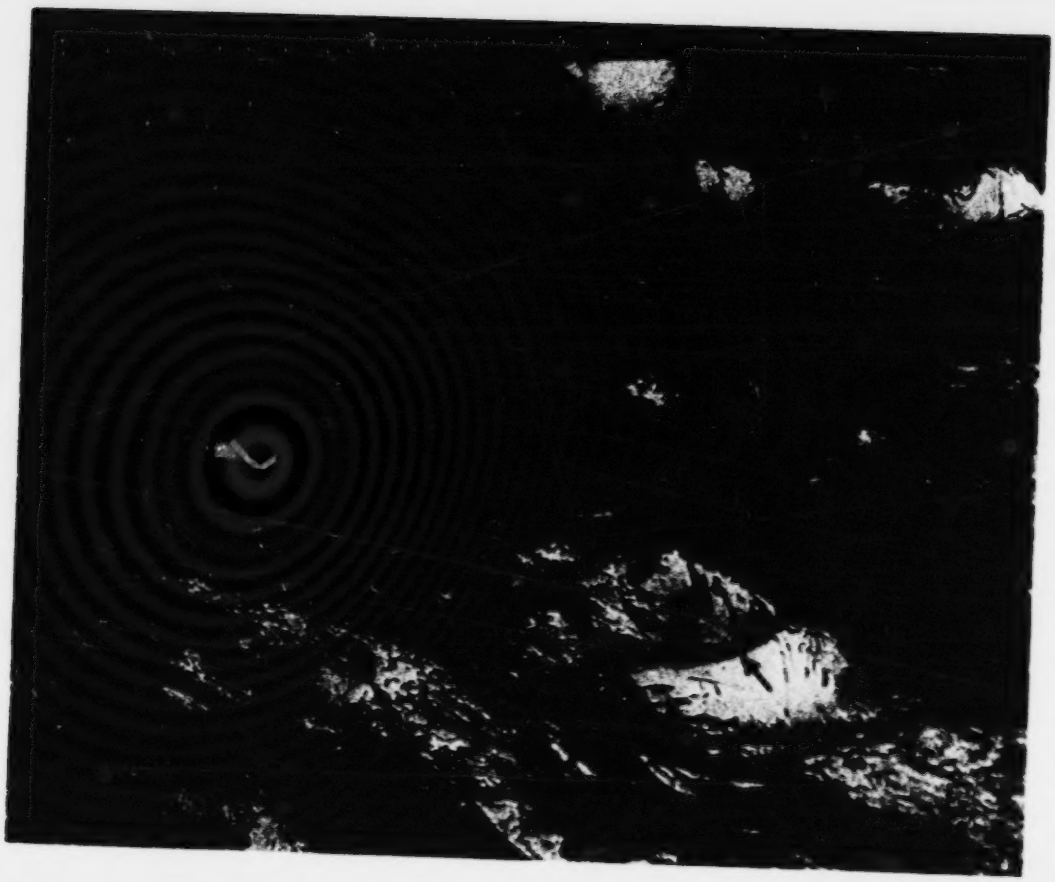

Fig. 8(j). Disk "12" (low rail). X500. Arrow points to crack associated with martensite. (neg 8349)

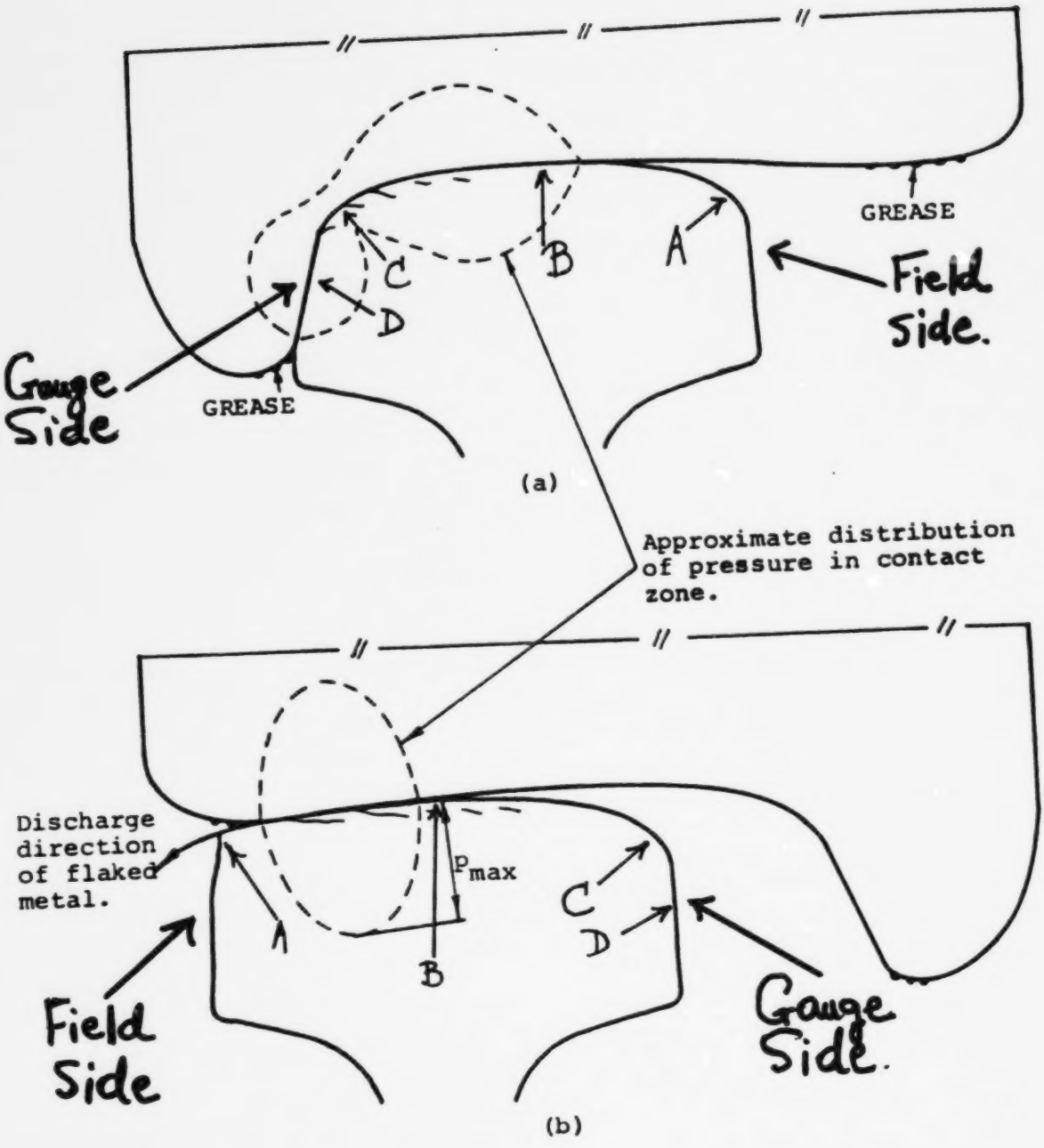

Fig. 9. Relative positions of wheel on rail during curve negotiation.
(a) high rail.
(b) low rail.